Noncollinear Andreev reflections in semiconductor nanowires

B. H. Wu,[1,*] W. Yi,[2,3,†] J. C. Cao,[4] and G.-C. Guo[2,3]

[1]*Department of Applied Physics, Donghua University, 2999 North Renmin Road, Shanghai 201620, China*
[2]*Key Laboratory of Quantum Information, University of Science and Technology of China, CAS, Hefei,*
Anhui 230026, People's Republic of China
[3]*Synergetic Innovation Center of Quantum Information and Quantum Physics, University of Science and Technology of China,*
Hefei, Anhui 230026, China
[4]*Key Laboratory of Terahertz Solid-State Technology, Shanghai Institute of Microsystem and Information Technology,*
Chinese Academy of Sciences, 865 Changning Road, Shanghai 200050, China

We show that noncollinear Andreev reflections can be induced at interfaces of semiconductor nanowires with spin-orbit coupling, Zeeman splitting, and proximity-induced superconductivity. In a noncollinear local Andreev reflection, the spin polarizations of the injected and the retro-reflected carriers are typically at an angle that is tunable via system parameters. While in a nonlocal transport, this noncollinearity enables us to identify and block, at different voltage configurations, the noncollinear cross Andreev reflection and the direct charge transfer processes. We demonstrate that the intriguing noncollinearity originates from the spin-dependent coupling between carriers in the lead and the lowest discrete states in the wire, which, for a topological superconducting nanowire, are related to the overlap-induced hybridization of Majorana edge states in a finite system. These interesting phenomena can be observed in semiconductor nanowires of experimentally relevant lengths, and are potentially useful for spintronics.

PACS number(s): 73.23.−b, 74.45.+c, 74.78.−w, 85.75.−d

I. INTRODUCTION

Andreev reflection (AR) plays a central role in the charge transmission at the interface between a normal conductor (N) and a superconductor (S) [1–3]. An important feature of the process is its spin dependence. For instance, near the interface, electrons with a certain spin injected from N are retroreflected as holes of the opposite spin via a conventional local Andreev reflection (LAR). When the spin flip is allowed at the interface, equal-spin AR can occur, where both the electrons and the holes have the same spin [4,5]. Recently, it has been shown that equal-spin AR can also be induced by the Majorana bound state (MBS) residing on the edge of a semi-infinite topological superconducting nanowire with spin-orbit coupling (SOC), Zeeman splitting, and proximity-induced superconductivity [6,7]. As the equal-spin AR therein originates from the self-Hermitian nature of MBS, the spin dependence of the AR is bound to be affected in finite-size systems, where overlap coupling between MBSs on different edges invalidates the self-Hermitian property.

More generally, for a finite-length nanowire with SOC, Zeeman splitting and proximity-induced superconductivity, pairs of nondegenerate discrete states appear in the energy spectrum [8,9]. In a finite-size topological superconducting wire, the lowest discrete states, i.e., the pair of states closest to the Fermi surface, correspond to the in-gap states induced by the hybridization of MBSs on the edges. While in a topologically trivial wire with finite length, the lowest discrete states correspond to the gap-edge states. In this work, we show that carriers involved in a resonant AR with the lowest discrete states can have noncollinear spin orientations, in contrast to the conventional and the equal-spin AR.

In a noncollinear LAR, the spin polarizations of the injected and retroreflected carriers are typically at an angle, tunable via system parameters. Hence LAR can be suppressed by using a half-metal (HM) lead whose carriers only have finite spin projections along one of the polarization directions. We show that the noncollinear AR is intimately connected to the local spin orientations of the lowest discrete states at the edge. Under appropriate parameters, the conventional or the equal-spin AR can be recovered as limiting cases of the more general noncollinear AR, which is particularly important for finite-size nanowires in realistic experiments.

This noncollinearity is particularly important for nonlocal transport processes where the wire length is typically comparable to the superconducting coherence length [10–19]. In general, when an electron is injected from one N lead to the S, it can either form a Cooper pair in the S and leave an out-going hole in the other N lead; or it can propagate through the S to the other lead. These two different processes respectively correspond to the cross Andreev reflection (CAR) [10,11] and the direct charge transfer [13]. By sandwiching the wire between two HM leads [see Fig. 1(a)], we show that, depending on whether the Fermi levels of the two leads are aligned with the same [Fig. 1(b)] or different [Fig. 1(c)] discrete states, these noncollinear nonlocal transport processes can be respectively blocked by adjusting the magnetization of the HM leads. The noncollinearity then provides us with a useful tool to selectively induce fully spin-polarized currents for applications in spintronics.

The paper is organized as follows: in Sec. II, we first introduce a model system where the noncollinear AR can be observed. Then, we present the effective Hamiltonian as well as our formalism based on nonequilibrium Green's functions to calculate the transport properties. In Sec. III, numerical results

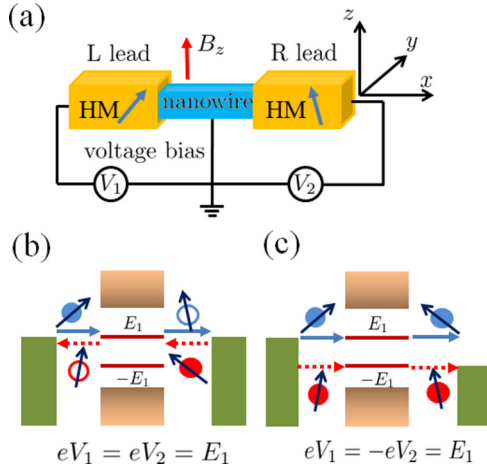*bhwu2010@gmail.com
†wyiz@ustc.edu.cn

FIG. 1. (Color online) (a) A semiconductor nanowire with proximity-induced superconductivity is coupled to two leads. Under different voltage configurations, either a resonant CAR (b) or a direct charge transfer (c) can occur. In either case, two different microscopic transport channels, marked by blue-solid and red-dashed lines respectively, exist, which are characterized by the electrons (filled circle) and holes (empty circle)in the leads with noncollinear spin polarizations (black arrows). The nonlocal transport processes can thus be blocked by adjusting the polarizations of the HM leads, such that transport in both microscopic channels become impossible.

based on realistic parameters of InSb nanowires are presented. We show that the noncollinearity can leave signatures in the differential conductance and the current noise, and that different microscopic processes in the LAR or the CAR can be selectively blocked. Finally, a brief summary is presented in Sec. IV.

II. MODEL AND FORMALISM

We consider a quasi-one-dimensional semiconductor nanowire, which can host MBS for appropriate parameters [20]. As illustrated in Fig. 1(a), the wire lies in the x direction with an external magnetic field B_z along the z direction. The two ends of the nanowire can be coupled, respectively, to the left (L) and the right (R) leads. The wire is grounded while the two leads are biased by applying voltages V_1 and V_2, respectively.

The tight-binding Hamiltonian of the nanowire [21,22]

$$H_{\text{wire}} = \sum_{j=1}^{N-1} \left(-\frac{t_0}{2} c_j^\dagger c_{j+1} - \frac{\alpha_{\text{SO}}}{2} i c_j^\dagger \sigma_y c_{j+1} + \text{H.c.} \right)$$

$$+ \sum_{j=1}^{N} [V_z c_j^\dagger \sigma_z c_j - (\mu - t_0) c_j^\dagger c_j + \Delta(c_{j\uparrow} c_{j\downarrow} + \text{H.c.})],$$

where $c_j = (c_{j\uparrow}, c_{j\downarrow})^T$ is electron annihilation operator in spinor form at site j with spin up ($\uparrow$) and down ($\downarrow$) in the z direction, N is the number of the lattice sites, $\sigma_{y,z}$ are the Pauli matrices, $\alpha_{\text{SO}} = \alpha_R/a$ is the SOC constant with the Rashba parameter α_R and the lattice spacing a, V_z is the effective Zeeman field, Δ is the proximity-induced superconducting gap, and μ is the chemical potential. The

hopping rate $t_0 = \frac{\hbar^2}{m^* a^2}$, with the effective mass of electrons m^*. The eigenspectrum of H_{wire} for a finite-size system consists of pairs of nondegenerate discrete states. We may then define the local spin orientation of a discrete state: $\vec{s}_{e/h}(x) = \frac{\langle \psi_{e/h}(x) | \vec{\sigma} | \psi_{e/h}(x) \rangle}{\langle \psi_{e/h}(x) | \psi_{e/h}(x) \rangle}$, which is useful for understanding the noncollinear AR. Here, $\vec{\sigma}$ is a vector of Pauli matrices and $\psi_{e/h}(x)$ is a spinor in the Nambu space for the electron (hole) component of the discrete state wave function.

The leads are described by the mean-field Stoner model [23]: $H_{\text{lead}} = \sum_{\alpha k s} \epsilon_{\alpha k s} a_{\alpha k s}^\dagger a_{\alpha k s}$, where $a_{\alpha k s}$ is the annihilation operator with quantum number k, spin index s and energy $\epsilon_{\alpha k s}$ in the $\alpha = $ L,R lead. Here, $s = +(-)$ denotes spins parallel (antiparallel) to the magnetic moment $\boldsymbol{n}_\alpha = (\sin\theta_\alpha \cos\varphi_\alpha, \sin\theta_\alpha \sin\varphi_\alpha, \cos\theta_\alpha)$, where θ_α and φ_α are the azimuthal angles in the α lead.

The coupling between the leads and the wire is spin conserving: $H_T = \sum_k (t_L c_1^\dagger u_L a_{Lk} + \text{H.c.}) + \sum_k (t_R c_N^\dagger u_R a_{Rk} + \text{H.c.})$, where t_α is the hopping between the α lead and the wire. The electron annihilation operators in spinor form $a_{\alpha k} = (a_{\alpha k+}, a_{\alpha k-})^T$. The unitary matrix u_α [24] accounts for the magnetic-moment misalignment in the α lead with the z direction

$$u_\alpha = \begin{pmatrix} \cos\theta_\alpha/2 & e^{-i\varphi_\alpha} \sin\theta_\alpha/2 \\ e^{i\varphi_\alpha} \sin\theta_\alpha/2 & -\cos\theta_\alpha/2 \end{pmatrix}.$$

The coupling strength between the wire and the α lead $\Gamma_\alpha^s = 2\pi |t_\alpha|^2 \rho_\alpha^s$ ($s = \pm$), which is energy independent in the wideband limit. Under the Stoner model, the spin asymmetry in the α lead is characterized by its density of states ρ_α^s for the majority ($s = +$) and minority ($s = -$) spins. For a normal lead, we have $\Gamma_\alpha^+ = \Gamma_\alpha^-$; while for HM leads, $\Gamma_\alpha^- = 0$.

We are interested in the transport properties of the system. The current operator for the L lead $\hat{I} = -e\dot{N}_L$ [25], with the carrier number $N_L = \sum_{ks} a_{Lks}^\dagger a_{Lks}$. Much information can be obtained from the current fluctuation or noise due to the discrete nature of the charge transport [26]. Here, we focus on the autocorrelation of the current from the L lead. The zero-frequency noise spectral density $S = \hbar \int dt' \langle \delta I(t') \delta I(0) + \delta I(0) \delta I(t') \rangle$, where $\delta I(t') = \hat{I}(t) - I$ with $I = \langle \hat{I} \rangle$ the direct current from the L lead. Both I and S can be evaluated by the standard Keldysh Green's function method [25].

The current from the L lead is given by

$$I = \frac{e}{h} \int d\epsilon \, \text{ReTr}\{\hat{\sigma}[\boldsymbol{G}^< \boldsymbol{\Sigma}_{1,1}^a + \boldsymbol{G}^r \boldsymbol{\Sigma}_{1,1}^<]\}, \quad (1)$$

where $\hat{\sigma} = \text{diag}(1, -1, 1, -1)$ in the spin⊗Nambu space accounts for the different charge carried by electrons and holes. The retarded (lesser) Green's function $\boldsymbol{G}^{r/<}$ can be derived from the analytical continuation of the contour-ordered Green's function $\boldsymbol{G}(t,t') = -i\langle T\psi(t)\psi^\dagger(t') \rangle$, where $\psi_j = (c_{j\uparrow}, c_{j\downarrow}^\dagger, c_{j\downarrow}, c_{j\uparrow}^\dagger)^T$. The retarded (advanced) self-energy $\boldsymbol{\Sigma}^{r/a}$ with the relation $\boldsymbol{\Sigma}^r = (\boldsymbol{\Sigma}^a)^\dagger$ has nonzero elements for lattice sites at the ends of the wire due to the tunnel coupling. In the wide-band limit, $\boldsymbol{\Sigma}^r$ for the outmost sites is given by $\boldsymbol{\Sigma}_{1,1}^r = -i\boldsymbol{\Gamma}_L/2$ and $\boldsymbol{\Sigma}_{N,N}^r = -i\boldsymbol{\Gamma}_R/2$, where the matrix $\boldsymbol{\Gamma}_\alpha$

is given in spin⊗Nambu space as

$$
\mathbf{\Gamma}_\alpha = \begin{pmatrix} \gamma_{11} & 0 & \gamma_{12} & 0 \\ 0 & \gamma_{22} & 0 & \gamma_{21} \\ \gamma_{21} & 0 & \gamma_{22} & 0 \\ 0 & \gamma_{12} & 0 & \gamma_{11} \end{pmatrix}.
$$

Here, $\gamma_{11} = \Gamma_\alpha^+ \cos^2 \frac{\theta_\alpha}{2} + \Gamma_\alpha^- \sin^2 \frac{\theta_\alpha}{2}$, $\gamma_{22} = \Gamma_\alpha^+ \sin^2 \frac{\theta_\alpha}{2} + \Gamma_\alpha^- \cos^2 \frac{\theta_\alpha}{2}$, $\gamma_{12} = (\Gamma_\alpha^+ e^{-i\varphi_\alpha} - \Gamma_\alpha^- e^{i\varphi_\alpha})\frac{\sin \theta_\alpha}{2}$, and $\gamma_{21} = \gamma_{12}^*$. The lesser self-energy $\mathbf{\Sigma}^<$, which characterizes the particle injection from the leads, is given by $\mathbf{\Sigma}^< = [\mathbf{\Sigma}^a - \mathbf{\Sigma}^r]\mathbf{F}$, where $\mathbf{F}_{1,1} = \text{diag}(f(\epsilon - \mu_L), f(\epsilon + \mu_L), f(\epsilon - \mu_L), f(\epsilon + \mu_L))$ and $\mathbf{F}_{N,N} = \text{diag}(f(\epsilon - \mu_R), f(\epsilon + \mu_R), f(\epsilon - \mu_R), f(\epsilon + \mu_R))$, with f being the Fermi distribution function.

In this work, we focus on the autocorrelation of the current from the L lead. The zero-frequency noise spectral density is defined as $S = \hbar \int dt' \langle \delta I(t') \delta I(0) + \delta I(0) \delta I(t') \rangle$, where $\delta I(t') = \hat{I}(t) - I$ is the current fluctuation. $\hat{I}$ is the current operator. In terms of the Green's functions and self-energies, the noise spectral density can be obtained from

$$
\begin{aligned}
S = \frac{e^2}{h} \int d\epsilon \, \text{Tr}\{ & [\hat{\sigma}\mathbf{\Sigma}_{1,1}^< \hat{\sigma}\mathbf{G}^> + \mathbf{G}^< \hat{\sigma}\mathbf{\Sigma}_{1,1}^> \hat{\sigma}] \\
& - \hat{\sigma}[\mathbf{\Sigma}_{1,1}\mathbf{G}]^< \hat{\sigma}[\mathbf{\Sigma}_{1,1}\mathbf{G}]^> - [\mathbf{G}\mathbf{\Sigma}_{1,1}]^< \hat{\sigma}[\mathbf{G}\mathbf{\Sigma}_{1,1}]^> \hat{\sigma} \\
& + \mathbf{G}^> \hat{\sigma}[\mathbf{\Sigma}_{1,1}\mathbf{G}\mathbf{\Sigma}_{1,1}]^< \hat{\sigma} + \hat{\sigma}[\mathbf{\Sigma}_{1,1}\mathbf{G}\mathbf{\Sigma}_{1,1}]^> \hat{\sigma}\mathbf{G}^< \}, \quad (2)
\end{aligned}
$$

where the Langreth theorem of analytic continuation such as $[AB]^{\lessgtr} = A^r B^{\lessgtr} + A^{\lessgtr} B^a$ and $[ABC]^{\lessgtr} = A^r B^r C^{\lessgtr} + A^r B^{\lessgtr} C^a + A^{\lessgtr} B^a C^a$, have been employed. In the above expressions, the advanced Green's function $\mathbf{G}^a = (\mathbf{G}^r)^\dagger$ and the greater Green's function $\mathbf{G}^>$ can be found from the relation $\mathbf{G}^> - \mathbf{G}^< = \mathbf{G}^r - \mathbf{G}^a$.

III. NUMERICAL RESULTS AND DISCUSSION

For numerical simulations, we consider a heterostructure at zero temperature where a InSb nanowire is in contact with NbTiN [27] or Ni [28], with the parameters: $m^* = 0.015m_e$, with m_e the electron mass, $\alpha_R = 0.25$ eV Å, $a = 1$ nm, and $\Delta \sim 140$ µeV. With these, we show that the noncollinear AR can occur in nanowires ranging from submicrometer to several microns in length.

A. Discrete states and local Andreev reflection

As the resonant AR is typically connected with discrete states in the wire, we focus on the lowest discrete states in a finite system, which, under the particle-hole symmetry, emerge as a pair with the same energy spacing E_1 to the Fermi energy. We show in Fig. 2 the nonmonotonic evolution of E_1 as a function of V_z [8,9]. These discrete states can be probed by the transport measurement. With an N lead coupled to one end of the wire, the dominant transport process is the LAR. When the Fermi level of the lead is aligned with E_1, conductance peaks of resonant LAR can be identified, where the peak value approaches $2e^2/h$, as shown in the inset of Fig. 2.

The spin dependence of LAR can be identified by replacing the N lead with an HM lead, while letting the bias voltage V satisfy the condition for a resonant AR. We plot the differential conductance dI/dV in Fig. 3(a) as a function of the azimuthal angles θ and φ of the HM magnetic moment. In most situations,
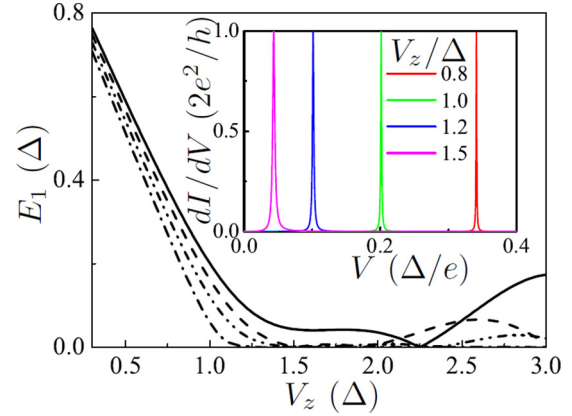

FIG. 2. (Color online) The lowest discrete state energy E_1 of the wire as a function of the effective Zeeman field V_z for wire length $L = 1.2$ (solid line), 1.5 (dashed line), 2.1 (dash dot dot line), and 4.5 µm (dash dot line). The inset: differential conductance dI/dV at various V_z. Parameters for the inset: $L = 1.2$ µm, $\Gamma_L^\pm = 0.2 \, t_0$.

dI/dV approaches $2e^2/h$ due to resonant LAR. However, two separate dips can be identified in Fig. 3(a), indicating the complete suppression of LAR at two particular magnetic moments of the HM lead. For an HM lead with a particular magnetic-moment alignment, carriers with spin opposite to that direction are blocked. Thus the existence of two dips in Fig. 3(a) suggests that carriers with spin opposite to the direction corresponding to either dip are intrinsic in the LAR process; that the LAR can be blocked when carriers with one of the two special spin polarizations become unavailable. Since the angle between these two spin polarizations is different from π (opposite-spin AR) and 0 (equal-spin AR), Fig. 3(a) clearly indicates a noncollinear LAR. The noncollinear LAR can also be revealed by the current noise Fano factor $F = S/2eI$ [26,29,30]. For the LAR-dominated transport, the Fano factor approaches 2 at low transmission, indicating an effective transfer of two electrons in the process [11]. In Fig. 3(b), two such peaks emerge in the contour plot of F, whose positions are consistent with those of the dips in Fig. 2(a).

As the coupling between the lead and the wire is spin conserving, it is instructive to explore the local spin orientation of the lowest discrete state in resonance [31]. In Fig. 4(a), we plot the spatial dependence of the angle $\Delta\theta$ between $\vec{s}_e$ and $\vec{s}_h$ of the lowest discrete state with energy E_1. While the spin orientations of electron and hole components are opposite ($\Delta\theta = \pi$) with vanishing α_R or V_z, they become spatially varying and noncollinear under finite SOC parameters, with $\Delta\theta$ at the wire end tunable over a wide range by adjusting α_R, V_z or L. In particular, in the topological superconducting regime, as L increases, $\Delta\theta$ approaches 0. This is consistent with the MBS-induced equal-spin AR in Ref. [6], where the spin orientations of electron and hole components of the MBS are the same due to the self-Hermitian nature of MBS. In a finite topological superconducting wire, the MBSs on different edges overlap to form the lowest discrete states, which acquire a finite $\Delta\theta$. A natural implication here is that the spin-dependence of AR should be intimately connected to the local spin orientation $\Delta\theta$ at the edges.
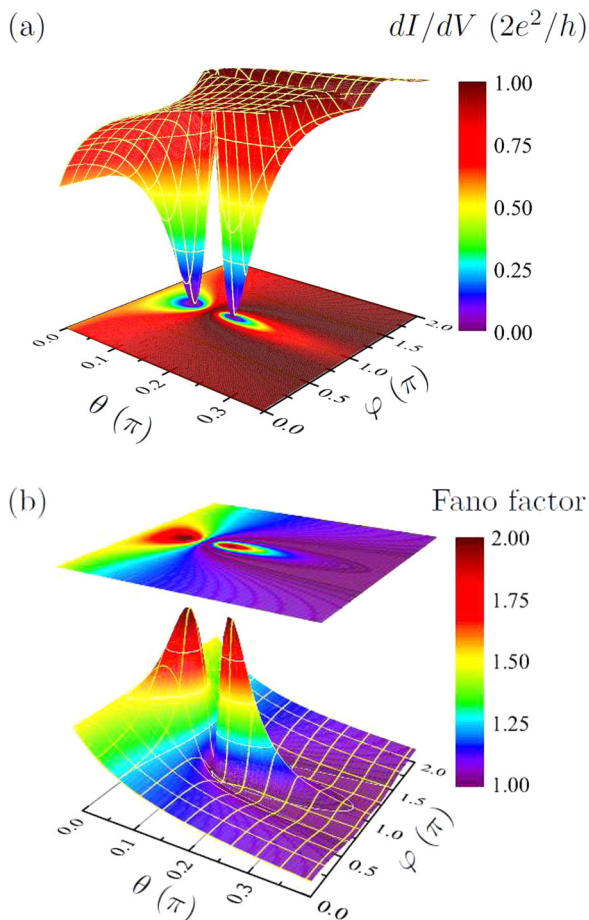
FIG. 3. (Color online) Contour plots of the differential conductance dI/dV (a) and noise Fano factor (b) due to the resonant LAR as functions of azimuthal angles θ and φ of the HM magnetic moment. Parameters: $V_z = 1.2\,\Delta$, $\Gamma_L^+ = 0.4\,t_0$, and $L = 1.2\,\mu\mathrm{m}$.

To see this, we vary the magnetic moment of the HM lead in the x-z plane, and adopt the convention: $\theta > 0$ for $\varphi = 0$; $\theta < 0$ for $\varphi = \pi$. Figure 4(b) displays the contour plot of dI/dV as a function of θ and V_z, for which the voltage $eV = E_1$. The directions opposing that of the local $\vec{s}_e(0)$ and $\vec{s}_h(0)$ at the wire end are also displayed with dashed lines. The overlap between the dashed lines and the dI/dV dips clearly indicates that resonant LAR can be suppressed once carriers with spin aligned with either $\vec{s}_e(0)$ or $\vec{s}_h(0)$ become unavailable in the lead.

B. Crossed Andreev reflection and direct charge transfer

The noncollinearity discussed in the previous subsection can also be manifested in the nonlocal transport with two leads [10–12,14,15], where the spin-polarization of the carrier passing through one N-S interface can take an arbitrary angle to that of the carrier at the other interface. Depending on the voltage configuration of the leads, nonlocal transport processes, such as the CAR and the direct charge transfer can be selectively blocked based on this noncollinearity.

We consider the typical case where two HM leads are symmetrically attached to two ends of the wire at $x = 0$ and $x = L$. The Hamiltonian of the wire observes the symmetry:
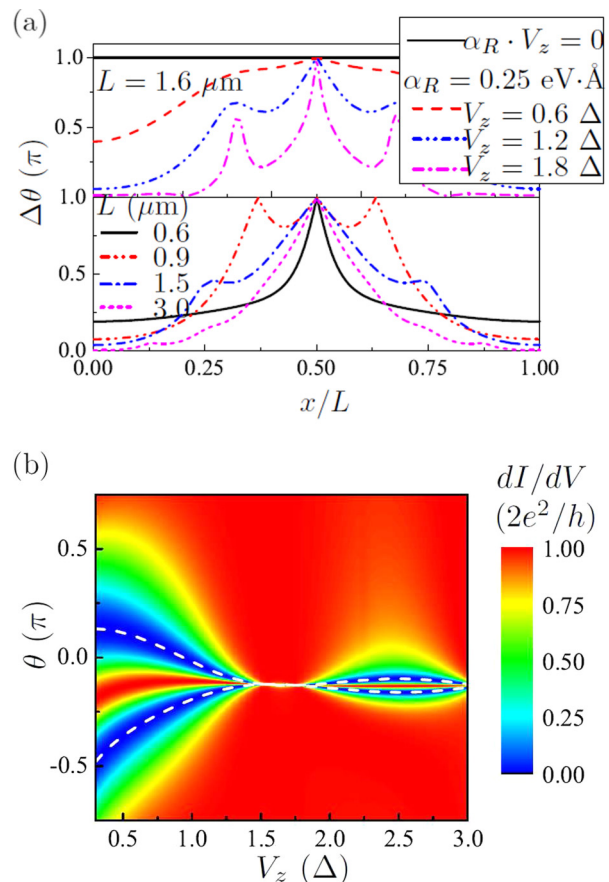

FIG. 4. (Color online) (a) The spatial dependence of $\Delta\theta$, the angle for the local spin orientations of the lowest discrete state in resonance, for varius V_z, α_R and L. (b) Contour plot of the differential conductance dI/dV as a function of V_z and the azimuth angle θ of the magnetic moment in the HM lead. The dashed lines in (b) indicate the directions opposing the local spin orientations of the lowest discrete state on the edge. Other parameters: $\Gamma_L^+ = 0.4\,t_0$, $V_z = 1.2\,\Delta$, $L = 1.2\,\mu\mathrm{m}$, and $\alpha_R = 0.25\,\mathrm{eV}\cdot\text{Å}$.

$H(x,\alpha) = H(L - x, -\alpha)$. For the discrete state with energy E_1, the local spin orientations satisfy: $s_{e/h}^{x,y}(x) = -s_{e/h}^{x,y}(L - x)$ and $s_{e/h}^z(x) = s_{e/h}^z(L - x)$.

We first consider identical bias voltages $eV_1 = eV_2 = E_1$, where the Fermi levels of both leads are aligned with the same discrete state [Fig. 1(b)]. The dominant nonlocal transport here is the CAR. As demonstrated in Fig. 5(a), by varying the spin orientations of the L and R leads in the x-z plane, two broad humps, each with a sharp feature peaking close to 2, appear in the noise Fano factor, indicating LAR-dominated low transmission. The locations of both peaks satisfy $\theta_L = -\theta_R$, representing either the simultaneous blocking of carriers with spins aligned in the $\vec{s}_e(0)$ direction at the left N-S interface and those with spins in the $\vec{s}_e(L)$ direction at the right interface; or the simultaneous blocking of carriers with spin aligned with $\vec{s}_h(0)$ at the left and those with spins in the $\vec{s}_h(L)$ direction at the right. The peaks thus indicate the simultaneous blocking of both microscopic transport channels illustrated in Fig. 1(b).

Next, we consider the bias voltages $eV_1 = -eV_2 = E_1$. The dominant nonlocal transport is then the direct charge transfer.
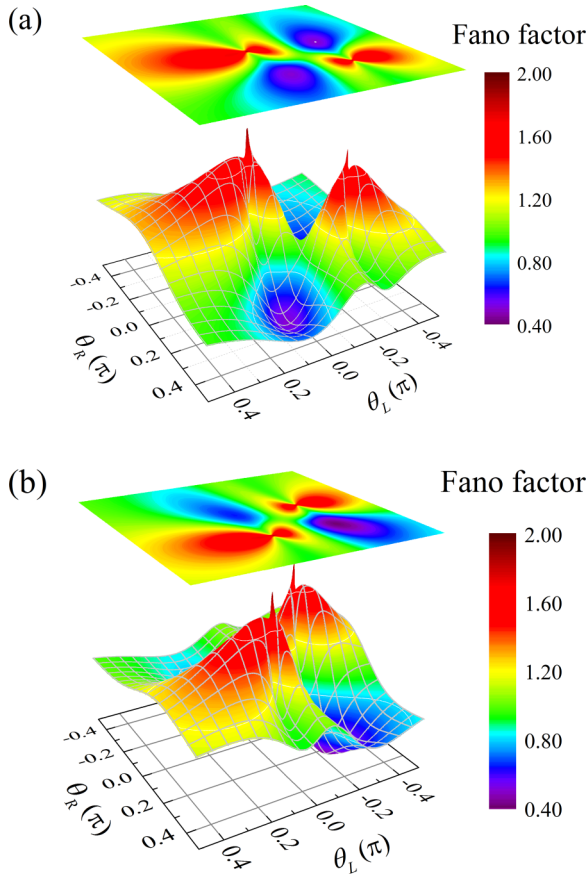
FIG. 5. (Color online) The contour plots of the noise Fano factor F as functions of θ_L and θ_R for different bias configurations for the resonant CAR: (a) $eV_1 = eV_2 = E_1$ and (b) $eV_1 = -eV_2 = E_1$. Parameters: $V_z = 0.8 \, \Delta$, $\Gamma_\alpha^+ = 0.4 \, t_0$, and $L = 1.2 \, \mu$m.

From the contour plot of the noise Fano factor at the L lead [Fig. 5(b)], we find two sharp peaks, with peak values close to 2. However, as $|\theta_L| \neq |\theta_R|$ at the peaks, they represent either the simultaneous blocking of carriers with spins in the $\vec{s}_e(0)$ direction at the left interface and those with $\vec{s}_h(L)$ at the right; or the simultaneous blocking of carriers with spins in the $\vec{s}_h(0)$ direction at the left and those with $\vec{s}_e(L)$ at the right [32]. The peaks thus indicate the simultaneous blocking of both microscopic transport channels in Fig. 1(c).

IV. CONCLUSION

We show that noncollinear AR can be induced at interfaces of semiconductor nanowires of finite, but experimentally relevant lengths. This feature provides us with a useful tool to induce fully spin-polarized current for applications in spintronics. The intriguing effects of noncollinear ARs can be observed in semiconductor nanowires with strong SOC, such as InSb [27,28] or InAs [33,34], which are currently under intensive study for the search of MBS. A test of the noncollinear AR via transport properties is also within the reach of current technology [35], where a supercurrent through HM films such as CrO_2 has recently been studied [36].

[1] A. F. Andreev, Sov. Phys. JETP **19**, 1228 (1964).

[2] G. E. Blonder, M. Tinkham, and T. M. Klapwijk, Phys. Rev. B **25**, 4515 (1982).

[3] M. Tinkham, *Introduction to Superconductivity*, 2nd ed. (Dover, New York, 2004).

[4] Z. P. Niu, Europhys. Lett. **100**, 17012 (2012).

[5] C. Visani, Z. Sefrioui, J. Tornos, C. Leon, J. Briatico, M. Bibes, A. Barthélémy, J. Santamaria, and J. Villegas, Nat. Phys. **8**, 539 (2012).

[6] J. J. He, T. K. Ng, P. A. Lee, and K. T. Law, Phys. Rev. Lett. **112**, 037001 (2014).

[7] J. J. He, J. S. Wu, T. P. Choy, X. J. Liu, Y. Tanaka, and K. T. Law, Nat. Commun. **5**, 3232 (2014).

[8] D. Rainis, L. Trifunovic, J. Klinovaja, and D. Loss, Phys. Rev. B **87**, 024515 (2013).

[9] T. D. Stanescu, R. M. Lutchyn, and S. Das Sarma, Phys. Rev. B **87**, 094518 (2013).

[10] J. Nilsson, A. R. Akhmerov, and C. W. J. Beenakker, Phys. Rev. Lett. **101**, 120403 (2008).

[11] K. T. Law, P. A. Lee, and T. K. Ng, Phys. Rev. Lett. **103**, 237001 (2009).

[12] J. Liu, F.-C. Zhang, and K. T. Law, Phys. Rev. B **88**, 064509 (2013).

[13] M. S. Kalenkov and A. D. Zaikin, Phys. Rev. B **75**, 172503 (2007).

[14] M. S. Kalenkov and A. D. Zaikin, in *Fundamentals of Superconducting Nanoelectronics*, edited by A. Sidorenko (Springer, Berlin-Heidelberg, 2011).

[15] J. Linder and A. Sudbø, in *Nanoscience and Engineering in Superconductivity*, edited by V. Moshchalkov, R. Wördenweber, and W. Lang (Springer, Berlin-Heidelberg, 2010).

[16] J. M. Byers and M. E. Flatté, Phys. Rev. Lett. **74**, 306 (1995).

[17] G. Deutscher and D. Feinberg, Appl. Phys. Lett. **76**, 487 (2000).

[18] M. S. Choi, C. Bruder, and D. Loss, Phys. Rev. B **62**, 13569 (2000).

[19] G. B. Lesovik, T. Martin, and G. Blatter, Eur. Phys. J. B **24**, 287 (2001).

[20] Y. Oreg, G. Refael, and F. von Oppen, Phys. Rev. Lett. **105**, 177002 (2010).

[21] E. M. Stoudenmire, J. Alicea, O. A. Starykh, and M. P. A. Fisher, Phys. Rev. B **84**, 014503 (2011).

[22] B. H. Wu and J. C. Cao, Phys. Rev. B **85**, 085415 (2012).

[23] Z. Y. Zeng, B. Li, and F. Claro, Phys. Rev. B **68**, 115319 (2003).

[24] J. C. Chen, S. G. Cheng, S. Q. Sun, and Q. F. Sun, J. Phys.: Condens. Matter **22**, 035301 (2010).

[25] H. Haug and A.-P. Jauho, *Quantum Kinetics in Transport and Optics of Semiconductors*, 2nd ed. (Springer, Berlin, 2008).

[26] Ya. M. Blanter and M. Büttiker, Phys. Rep. **336**, 1 (2000).

[27] V. Mourik, K. Zuo, S. M. Frolov, S. R. Plissard, E. P. A. M. Bakkers, and L. P. Kouwenhoven, Science **336**, 1003 (2012).

[28] M. T. Deng, C. L. Yu, G. Y. Huang, M. Larsson, P. Caroff, and H. Q. Xu, Nano Lett. **12**, 6414 (2012).

[29] D. Averin and H. T. Imam, Phys. Rev. Lett. **76**, 3814 (1996).

[30] J. C. Cuevas, A. Martín-Rodero, and A. Levy Yeyati, Phys. Rev. Lett. **82**, 4086 (1999).

[31] D. Sticlet, C. Bena, and P. Simon, Phys. Rev. Lett. **108**, 096802 (2012).

[32] Note the particle-hole symmetry dictates that the electron- (hole-) component spin polarizations of the E_1 state are identical to the hole- (electron-) component spin polarizations of the $-E_1$ state.

[33] A. Das, Y. Ronen, Y. Most, Y. Oreg, M. Heiblum, and H. Shtrikman, Nat. Phys. **8**, 887 (2012).

[34] E. J. H. Lee, X. Jiang, M. Houzet, R. Aguado, C. M. Lieber, and S. De Franceschi, Nat. Nanotechnol. **9**, 79 (2014).

[35] M. Colci, K. Sun, N. Shah, S. Vishveshwara, and D. J. Van Harlingen, Phys. Rev. B **85**, 180512(R) (2012); K. Sun, N. Shah, and S. Vishveshwara, *ibid.* **87**, 054509 (2013).

[36] R. S. Keizer, S. T. B. Goennenwein, T. M. Klapwijk, G. Miao, G. Xiao, and A. Gupta, Nature (London) **439**, 825 (2006).